ADVANCED MATERIALS
www.advmat.de

Localized Self-Growth of Reconfigurable Architectures Induced by a Femtosecond Laser on a Shape-Memory Polymer

Yachao Zhang, Ying Li, Yanlei Hu, Xuelin Zhu, Yaowei Huang, Zhen Zhang, Shenglong Rao, Zhijiang Hu, Weixin Qiu, Yulong Wang, Guoqiang Li, Liang Yang, Jiawen Li, Dong Wu,* Wenhao Huang, Chengwei Qiu,* and Jiaru Chu*

Architectures of natural organisms especially plants largely determine their response to varying external conditions. Nature-inspired shape transformation of artificial materials has motivated academic research for decades due to wide applications in smart textiles, actuators, soft robotics, and drug delivery. A "self-growth" method of controlling femtosecond laser scanning on the surface of a prestretched shape-memory polymer to realize microscale localized reconfigurable architectures transformation is introduced. It is discovered that microstructures can grow out of the original surface by intentional control of localized laser heating and ablation, and resultant structures can be further tuned by adopting an asymmetric laser scanning strategy. A distinguished paradigm of reconfigurable architectures is demonstrated by combining the flexible and programmable laser technique with a smart shape-memory polymer. Proof-of-concept experiments are performed respectively in information encryption/decryption, and microtarget capturing/release. The findings reveal new capacities of architectures with smart surfaces in various interdisciplinary fields including anti-counterfeiting, microstructure printing, and ultrasensitive detection.

Diverse natural organisms have fully evolved to possess the ability to change their shapes in response to external stimuli.[1–6] Examples of these shape transformation include opened seed-bearing pine cones when drying induced by differential swelling of two layers of scales,[1] symmetrical contraction-induced lengthening of octopus skin papilla when meeting predators,[5] heliotropism of sunflowers caused by differential lateral stem growth when exposed to directional sunlight.[7] Inspired by these natural behavior, many works have been done to realize reconfigurable shape transformation with artificial soft materials in a controlled manner.[8–11] Heterogeneous structures composited of hydrogel constituents with different swelling/shrinkage ratio[12–16] or anisotropic swelling behavior[17,18] have been constructed to accomplish dynamic tunable morphologies. Large shape deformation is shown in photodeformable crosslinked liquid crystal polymer through the orientation change of liquid crystal molecules,[19–22] and thus light-driven movable microarchitecture can be obtained. Inflation of elastic polymers constrained by relative stiff materials are applied to realize reconfigurable shape transformation.[23–25] These aforementioned shape reconfigurable materials are highly desired for many applications in soft robotics,[23,24] smart textiles,[26] drug delivery,[27] self-shaping devices,[28] and actuators.[22,29]

Although nature-inspired artificial dynamic architectures have been widely studied as referred above, so far most of the shape transformation are dependent on the whole material deformation due to the technical challenge to locally induce shape change in a bulk material. Efforts have been taken to achieve dynamic structural behavior such as self-folding through modification of the localized properties of active materials, but these can only be done in macroscale by embedding

Y. Zhang, Prof. Y. Hu, Z. Zhang, S. Rao, Z. Hu, W. Qiu, Y. Wang, Prof. G. Li, Dr. L. Yang, Prof. J. Li, Prof. D. Wu, Prof. W. Huang, Prof. J. Chu
CAS Key Laboratory of Mechanical Behavior and Design of Materials
Department of Precision Machinery and Precision Instrumentation
University of Science and Technology of China
Hefei, Anhui 230027, China
E-mail: huyl@ustc.edu.cn; dongwu@ustc.edu.cn

Dr. Y. Li, Dr. Y. Huang, Prof. C. Qiu
Department of Electrical and Computer Engineering
National University of Singapore
4 Engineering Drive 3, Singapore 117583, Singapore
E-mail: eleqc@nus.edu.sg

The ORCID identification number(s) for the author(s) of this article can be found under https://doi.org/10.1002/adma.201803072.

DOI: 10.1002/adma.201803072

Dr. X. Zhu
Centre for Micro and Nanoscale Research and Fabrication
University of Science and Technology of China
Hefei, Anhui 230027, China

Dr. Y. Huang
John A. Paulson School of Engineering and Applied Science
Harvard University
Cambridge, MA 02138, USA

Prof. G. Li
Key Laboratory of Testing Technology for Manufacturing Process of Ministry of Education
Southwest University of Science and Technology
Mianyang 621010, China

resistive circuits[28] or patterning heat absorption region.[30–32] Therefore, microscale localized shape transformation with high controllability and reconfigurability remains an ultimate challenge. In this regard, both "materials" and "technologies" need to be deliberately reconsidered. Shape-memory polymers (SMPs) are smart materials that can recover their predefined shape in response to external stimuli, and have been successfully applied in soft robot,[33] microfluidic chips,[34] ultrasensitive biosensors,[35] and cell and tissue engineering.[36] Meanwhile, laser is a powerful tool for treating materials with advantages of noncontact, high spatial precision, and flexibility. Although rarely reported, the combination of the superior deformability of shape-memory polymer and laser precise processing technology will bring new possibilities for realizing microscopic local shape transformation.

Herein, we utilize just a single homogeneous piece of low-cost shape-memory polystyrene film to realize microscale localized morphologies with reversible architectures, assisted with judiciously controlled femtosecond laser scanning strategies to launch symmetrical and asymmetrical growth. Fine self-growing, bending, and straightening effects are experimentally pronounced to construct reconfigurable architectures in situ tuning by adopting different laser writing fashions. Therefore, a variety of surface patterns can be fabricated, tuned and revert to uniform surface. To further capture the physics of the process, a shrinkage–growth model is proposed for this laser-induced polymer self-growing (LIPS) process and the bending/recovery process. Last but not least, proof-of-concept applications in various fields are presented to show promising interdisciplinary values of our findings.

The shrinkage properties of polystyrene film: As schematically depicted in **Figure 1**a, the polystyrene film severely shrinks when heated by a hot air gun. The film retracts to 45% of its original size in x–y plane, and increases by four times in z-direction (original thickness of the polystyrene film is ≈300 µm, and becomes ≈1500 µm after complete shrinkage, as shown in inset of Figure 1a). The shrinkage of SMP film in oven is shown in Figure S1a of the Supporting Information. The shrinkage property of polystyrene film is investigated at different temperatures in the oven as shown in Figure 1b. When the temperature (130 and 110 °C) exceeds glass transition temperature (T_g ≈ 107 °C), the film can achieve a maximum constant shrinkage ratio of 55% (Figure S1b, Supporting Information) while the film shrinks incompletely with the temperature (90 °C) below the T_g. In order to investigate the absorption mechanism, the UV–vis absorption spectrum of the polystyrene film is measured (Figure 1c). The film has strong absorption between 200 and 300 nm, implying that multiphoton ($n \geq 3$) absorption plays a dominant role under the irradiation of femtosecond laser with the wavelength of 800 nm.

LIPS of polystyrene film: mechanism of micropillar formation: Femtosecond laser machining has a finely confined

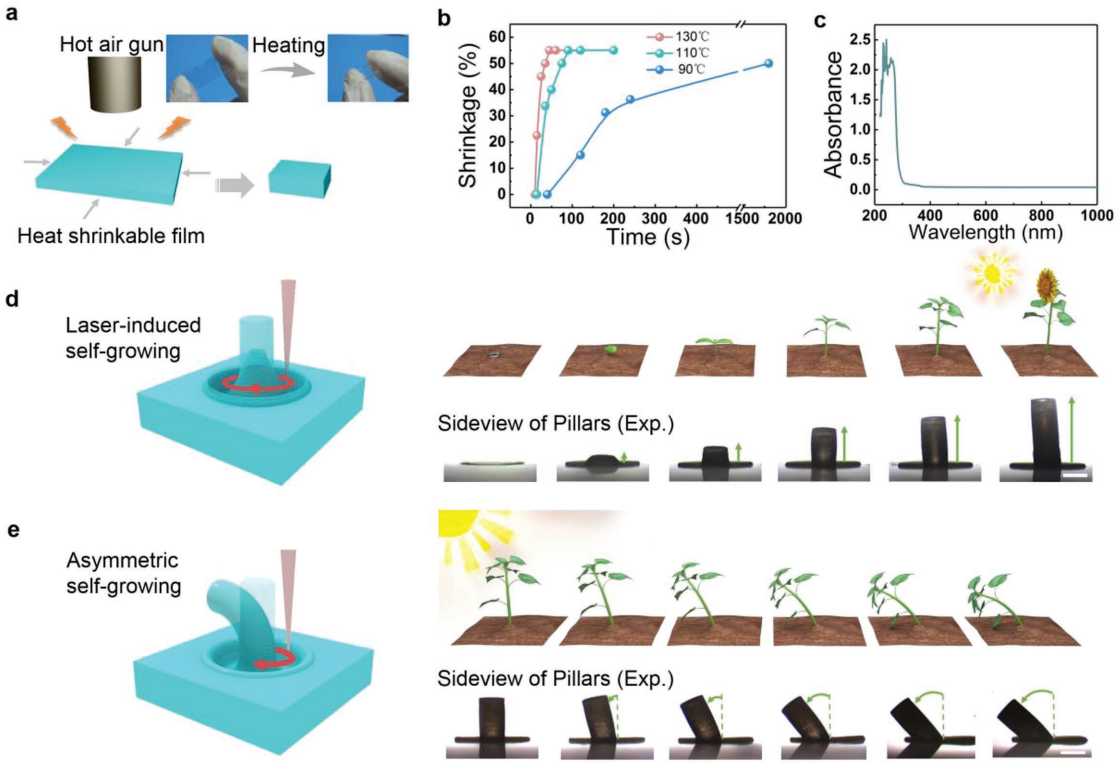

Figure 1. Shrinkage properties of polystyrene film and laser-grown smart structures mimicking sunflower. a) Schematic of heat-induced shrinkage of SMP film by a hot air gun. Inset: pictures of polystyrene film before and after heating. b) Dependence of shrinkage ratio of polystyrene film on the heating time at different temperatures (130, 110, and 90 °C). c) UV–vis absorption spectra of polystyrene film. d) Schematic of femtosecond laser processing SMP film. The red circle indicates the laser scanning path. Optical images show the growth of pillars with increasing repeat circles corresponding to the growth of sunflower. e) Schematic of femtosecond laser fabricating bent micropillar. The red semicircle indicates the laser scanning path. Optical images show the bending process of pillars with increasing repeat semicircles corresponding to the heliotropism of sunflower. Scale bars: 200 µm.

heat-affected zone with sufficiently high temperature, benefiting the localized manipulation of the polystyrene film. Here, a femtosecond laser writing setup as schematically illustrated in Figure 1d is employed to treat the polystyrene film. During the fabrication process, the laser is focused on the surface of sample and move along the preprogramed 2D routes. It is fascinating that a micropillar grows up when a repeated circular scanning path ranging from 1 to 80 circles is utilized, corresponding to the basic growth of sunflower as shown in Figure 1d. Like the sunflower can bend to the sun, the fabricated straight micropillar can bend when laser scan another semicircular path as shown in Figure 1e.

The interaction between laser and polystyrene film involves laser ablation and laser heating, which take place simultaneously during the micropillar formation. To fully understand the formation of micropillar, different numbers of repeat circles (ranging from 1 to 80) with the same diameter (470 μm) are employed and the corresponding micropillars are observed (Figure S2, Videos S1 and S2, Supporting Information).

According to the morphology of microstructure (**Figure 2**a (middle column); Figure S2, Supporting Information), the growth of micropillar can be divided into four stages with the increase of repeat circles, which is schematically sketched in Figure 2a (left column). In the first stage, ablation process happens, and the heat accumulation is not enough to induce the shrinkage. In the second stage, an inversed-bowl-shaped structure is gradually formed. The part near the upper surface shrinks much more than the bottom, while the central part of the scanning path has not shrunk and keeps flat, resulting in the inversed-bowl-shaped structure. In the third stage, a crater-shaped structure is formed, because as laser ablation deepens, the surface part further shrinks while the central part just reaches the glass transition temperature and starts to shrink. In the fourth stage, due to the further accumulation and conduction of heat, the temperature of the entire region inside the circular scanning path is high enough to trigger phase transition. Thus, the shrinkage in the x–y plane continues and with a growth in the z-direction. Eventually, the top layer shrinks completely and recovers flat. As the laser ablates deeper, the deeper layer shrinks completely. Therefore, this can be regarded as a layer-by-layer shrinking process and all layers shrink with the same degree, so the micropillar grow parallel up as a cylinder.

A comparative experiment between intermittent and continuous scanning is performed to demonstrate the dominant role of laser-induced thermal accumulation for the micropillar formation (Figure S3, Supporting Information). It should be noted that the laser power must be high enough to ablate the material and separate the structure from the matrix part in the x–y plane, otherwise just a bump can be induced.[37] It has also been revealed that the top of the micropillar has been completely thermally treated by laser and the root is only partly heated due to the distance from the focus (Figure S4, Supporting Information). To further understand the stages of the LIPS process, we develop an improved shrinkage–growth model based on Wayne's polyester shrink model[38] and Khonakdar's model.[39] Since that the volume of film is changed slightly after heating (Figure S1b, Supporting Information), we introduce a chamber filled with liquid, thus the heat-induced shrinkage of the SMP film in 3D can be well explained. As shown in Figure 2a (right column), the model is composed of three Kelvin units (the spring, S_1, S_2, S_3 and the dashpot, D_1, D_2, D_3 in parallel, respectively) and a chamber filled with liquid indicated with light blue. η is the viscosity of dashpot ($\eta_1 = \eta_2 = \eta_3$), and all the springs are assumed to have the same elastic properties.

For this model, four steps correspond to the four stages of the micropillar growth. Prior to step I, the Kelvin unit is stretched at high temperature where all the dashpots are in liquid state. The viscosity of the three dashpots is low at this temperature so Kelvin unit can stretch easily. Due to the change in chamber volume, the Kelvin unit in z-direction is compressed. Then in step I at room temperature, the extended spring S_1, S_2, and the compressed spring S_3 are frozen owing to the high viscosity of the dashpots, thus the film keeps the shape. In step II, η_1 and η_2 decrease as the temperature is raised by laser heating, while η_3 is still high because of the low temperature in the center. Thus, the extended spring S_1 and S_2 start to retract and S_3 is kept compressed and the film is partially contractive (in step II and III one Kelvin unit is employed at the center to simplify the model, details please refer to Figure S5, Supporting Information). Under further laser heating, the temperature of the central part reaches the glass transition temperature and the dashpot D_3 is in liquid state. In this stage, S_1 and S_2 continue retracting and S_3 starts to extend (step III). In step IV, the dashpot D_3 is in liquid state so that the spring S_3 can extend continuously. At last, all the three springs reach a balance length.

Microarchitectures under various laser parameters: Figure 2b–d shows the quantitative relationship between laser parameters and the morphology of the microstructure (the site we measure the diameter and length is shown in Figure 2a). The red curves are utilized to indicate that there is micropillar formed (stage IV) while blue curves mean that no micropillar is formed (stage I–III). The diameter of the microstructure is obviously influenced by the laser power, scanning speed, and repeat circles (Figures S6 and S7, Supporting Information). When the repeat circles and laser power increase, the microstructure diameter decreases because of the higher extent of shrinkage. As indicated by the red circle in Figure 2b–d, the smallest diameter of the microstructure top is 168.94 μm (Figure 2b), 167.75 μm (Figure 2c), and 169.15 μm (Figure 2d), respectively, which are smaller than the shrink limit indicated by the dashed lines (210 μm, calculated by the designed diameter of circular scanning path ≈470 μm and the maximum shrinkage ratio of 55%) owning to the temperature gradient causes inconsistent shrinkage in the radial direction described in the third stage. The diameter is finally stabilized at ≈210 μm coinciding with the macroscale shrinkage ratio limit of 55%. As the scanning speed increases (Figure 2d), the heating time of laser spot along the scanning path is decreased, which means that the whole energy provided by laser decreased at fixed laser power and repeat circles, the diameter firstly decreases beyond the shrink limit and then increase to the designed diameter of circular scanning path. Accordingly, the length increases with the repeat circles and laser power, and decreases with the scanning speed as shown in Figure 2b–d. As for the stage IV, the volume of micropillar has a well fitted linear relationship with repeat circles, power and reciprocal of the scanning speed

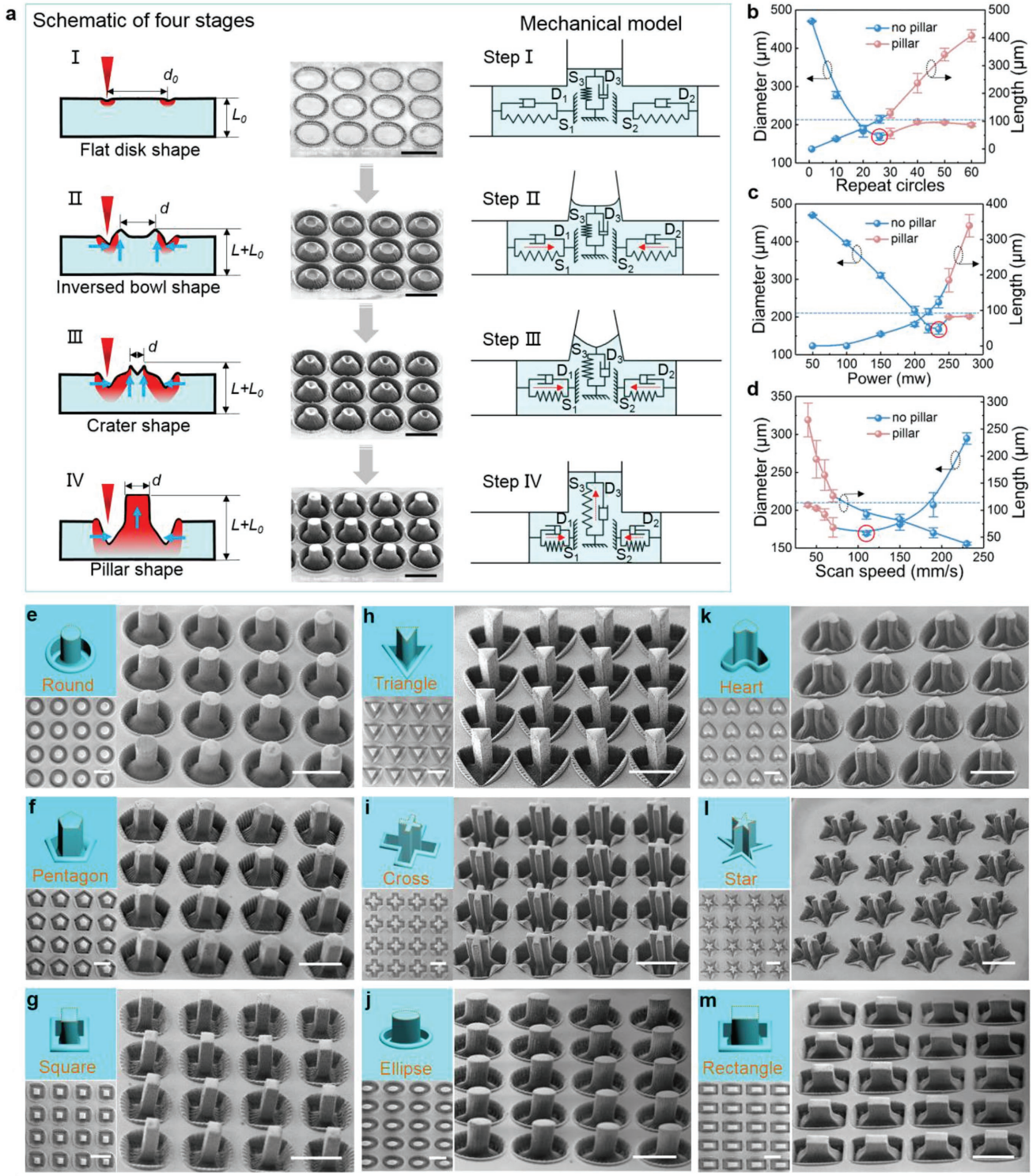

Figure 2. Shrinkage–growth model of laser-induced self-growing and diverse examples of laser-grown micropillars. a) Four stages during laser-induced polymer self-growing. I–IV: The schematics of cross-sectional profile of microstructure. SEM images in the middle column show corresponding microstructures (45°-titled view). Right columns show the evolving shrinkage–growth model of laser localized heating and scribing correspond to the four stages of the schematic. Blue arrows in the sketch indicate the shrink direction of material in *x*–*y* plane and increase direction in *z*-direction. Red color schematically indicates the distribution of temperature which is higher than the film glass transition temperature. Scale bars: 500 μm. b–d) The quantitative relationship between diameter and length of the microstructure with repeat circles, power, and scanning speed. Blue dot lines in (b)–(d) indicate the micropillar diameter with the macroscale maximum shrinkage limit of 55%. Red curves indicate that there are micropillar formed (stage IV) while blue curves mean no micropillar is formed (stage I–III). e–m) 45°-tilted view SEM images of round, pentagon, square, triangle, cross, ellipse, heart, star, and rectangle shape micropillars, respectively. Left columns show the corresponding top-view SEM images and schematics. All scale bars: 500 μm.

(Figure S8, Supporting Information). The fabrication resolution of LIPS is mainly determined by the focal length of *f*-theta lens and laser processing parameters including laser wavelength, power, and scanning speed. The smaller the wavelength and focal length of *f*-theta lens are, the smaller the laser focus spot is, resulting in higher spatial resolution. Using the processing parameters mentioned above, the relationship between the designed diameter and formed microstructure is investigated as shown in Figure S9 of the Supporting Information, the spatial resolution is 306.59 μm and the minimum diameter of the self-grown pillar is 149.62 μm (feature size). Due to the low thermal conductivity of the polymer, large single pattern cannot be fabricated and the maximum available pattern size is 473.07 μm according to our experiments (Figure S9, Supporting Information).

Owing to the flexibility of femtosecond laser writing, the position of micropillar and scanning path can be highly controlled. Various 2D geometrical patterns are employed to fabricate diverse micropillars (Figure 2e–m). Good geometry fidelity of cross-sections can be obtained by the proposed LIPS method.

Highly controllable bent micropillar formed by asymmetric LIPS (ALIPS): Besides the straight pillars, an asymmetric scanning strategy is adopted to fabricate bent micropillars. As schematically shown in **Figure 3**a, after a straight micropillar is formed, additional semicircular path (as indicated by blue) is scanned repeatedly on one side of the micropillar to generate asymmetric growth. Strain difference is induced in the partially scanned area, micropillar thus bends to the other side which is not heated (Video S3, Supporting Information). So far, we have successfully fabricated straight and bent micropillars on the prestretched polystyrene film. As for relaxed polystyrene film, laser scan continuously on the surface with the same parameters but just material ablation happened, indicating that the shape-memory effect enables the micropillar formation (Figure S10, Supporting Information).

To interpret the bending mechanism, the shrinkage–growth model described in Figure 2a is extended to a straight-bent model by introducing one more Kelvin unit (spring S_4 and dashpot D_4) as shown in Figure 3b,c. As the laser scanning the semicircular path repeatedly, the temperature rises quickly, both the dashpot D_2 and D_4 are in liquid state. The temperature from the heating side to the other side decrease gradually so the viscosity of dashpot D_4 decrease much more than dashpot D_3 and the viscosity of dashpot D_1 is still high. Since the spring S_2 retracts and the spring S_1 keeps still, the volume of the chamber starts to change. Therefore, the spring S_3 and S_4 extend with different degree and bend the micropillar.

We experimentally investigate the quantitative relationship between laser parameter and the morphology of the bent micropillar (Figure 3d,e). We first fabricate the straight pillar, and then control the repeat semicircles and its scanning speed at fixed power of 250 mW (Figure S11, Supporting Information). The bending angle (θ, the site we measure the angle is shown in Figure 3a) and length decrease with the scanning speed while increase with repeat semicircles (Figure 3d,e; Video S4, Supporting Information), since the heating time increases with slower scanning speed and more repeat semicircles.

Based on the understanding of bending mechanism and experiment, fabrication parameters are optimized to realize bent micropillars (Figure 3f). As shown in Figure 3g–m, the pillars number, spatial location, and bending direction can be easily controlled, leading to a variety of ordered patterns by using the bent micropillar as a basic unit. Larger scale patterns like Chinese knot and characters "people" are fabricated as shown in Figure 3n,o. Two patterns inspired by petal are fabricated with the same parameters (Figure 3p).

Due to the localized heating, the shape-memory capability can be utilized many times arbitrarily during micro/nanofabrication. We can not only bend the micropillar, but also allows the bent micropillars recover to straight or even bend in the opposite direction like the sunflower sway east to west during the day. The in situ tuning ability of our method is schematically shown in **Figure 4**a. We first fabricate a straight pillar, then scribe the blue arc path intermittently to preseparate the left root of the micropillar from the matrix. Next, we scribe the purple semicircular path at the right root of the micropillar continuously to bend the micropillar to left. To make the bent micropillar recover to straight, we scribe red arc path on the left side of the micropillar continuously, heat conduct to the prescribed area and induce the recovery process (details please refer to Figure S12, Supporting Information). Finally, we scribe the purple semicircle at the left root of the micropillar to make the micropillar bend to right. SEM images in Figure 4b show the bending angle of micropillar is tuned from 140° to 30°. Furthermore, the claw-like structure in Figure 4c can be tuned from close state to open state (Figure 4d–f), demonstrating high controllability of our method.

Applications of ALIPS prepared structures: Here we explore the possible applications of ALIPS in microparticle capture and information encryption. The assembled "four-pillar" structures (Figure 3j) provide a confined space between these pillars. As schematically shown in **Figure 5**a, the claw-like structure is fabricated around a microsphere and the "finger" grasps the microsphere tightly (Figure S13 and Video S5, Supporting Information) which can withstand a certain degree of shaking and external force. To release the microsphere, we can employ the strategy show in Figure 4a that the pillars are bent to opposite directions with additional asymmetric scanning. We can also place the sample in an ultrasonic cleaner with vibration for 10 min. The empty claw-like structure after the microsphere releasing is shown in Figure 5b.

Another particle-releasing method is to simply heat the sample with the hot air gun. The bent micropillar recover to straight and retract into the hole (Figure 5c; for details see Figure S14, Supporting Information), the microsphere is exposed on the surface and released at the same time. A bend-recovery model is put forward to explain the transformation (Figure 5d). On the one hand, the bent pillar recovers to straight since the side which is not additionally heated by laser still has the shrink capability and the strain difference caused by asymmetric laser scanning is resolved. On the other hand, the matrix material around the micropillar shrinks and increases its size in *z*-direction. Therefore, it seems that the micropillar retract back to the hole. According to the experiment, microspheres with different diameters and multiple microspheres can also be successfully captured by using the new type micromechanical hand (Figure S15, Supporting Information).

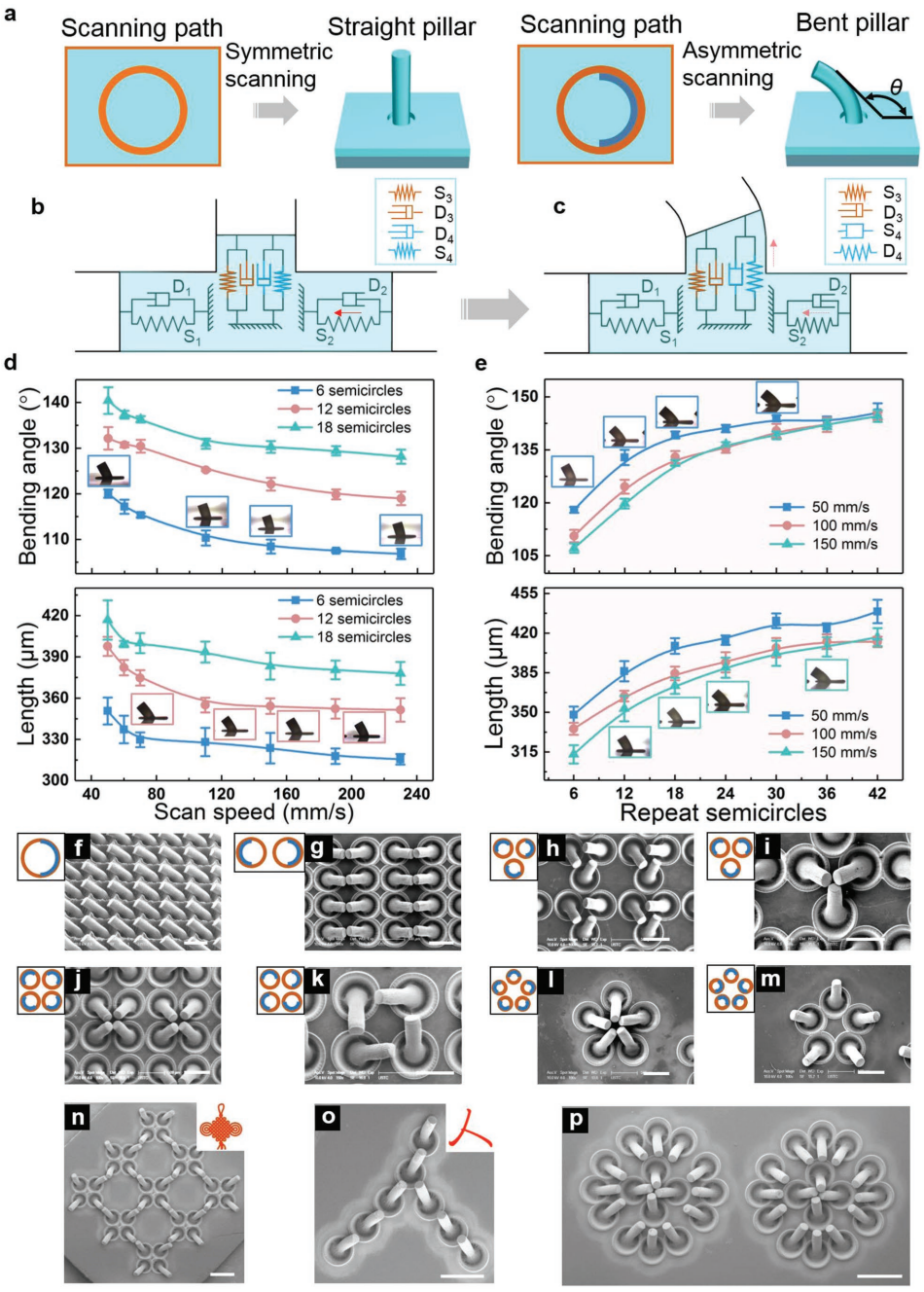

Figure 3. Fabrication of highly controllable bent micropillars. a) Schematic of the different scanning strategies for straight and bent micropillar fabrication. The lines with different colors indicate scanning path and scanning sequence. First the laser scribe along the orange pattern to form the straight micropillar, then along the blue pattern to bend the micropillar. b,c) The proposed straight-bent model. d) The quantitative relationship between bending angle and length of the micropillar with scanning speed at 6, 12, 18 semicircles. e) The quantitative relationship between bending angle and length of the micropillar with repeat semicircles at 50, 100, 150 mm s^{-1}. The site we measure the bending angle is shown in (a). f) Array of bent micropillars with the same bending direction. g) Two micropillars contacting each other on their tips by scanning the semicircle face to face as shown in the corresponding schematic. h) Three micropillars bending along the sides of the triangle. i) Three micropillars bending to the center of the triangle. j) Four micropillars bending to the center of the square. k) Four micropillars bending along the sides of the square. l,m) Five micropillars fabricated with both inward and outward directions, mimicking petals of closure and bloom of flowers. n–p) Large scale assemblies composed of bent micropillars. (n) Chinese knot. (o) Chinese characters "people." (p) Two patterns inspired by petal are fabricated with the same parameters. Scale bars: 500 μm (f)–(m), 1 mm (n)–(p).

Our method also offers a way for information-image encryption. The encryption–decryption process can be divided into three stages (Figure 5e). Square upright pillar is first fabricated on the ink QR code to discretize the information. One part of ink on the top of the pillar grows out of the surface. Another part of ink on the scanning path vanishes due to the ablation.

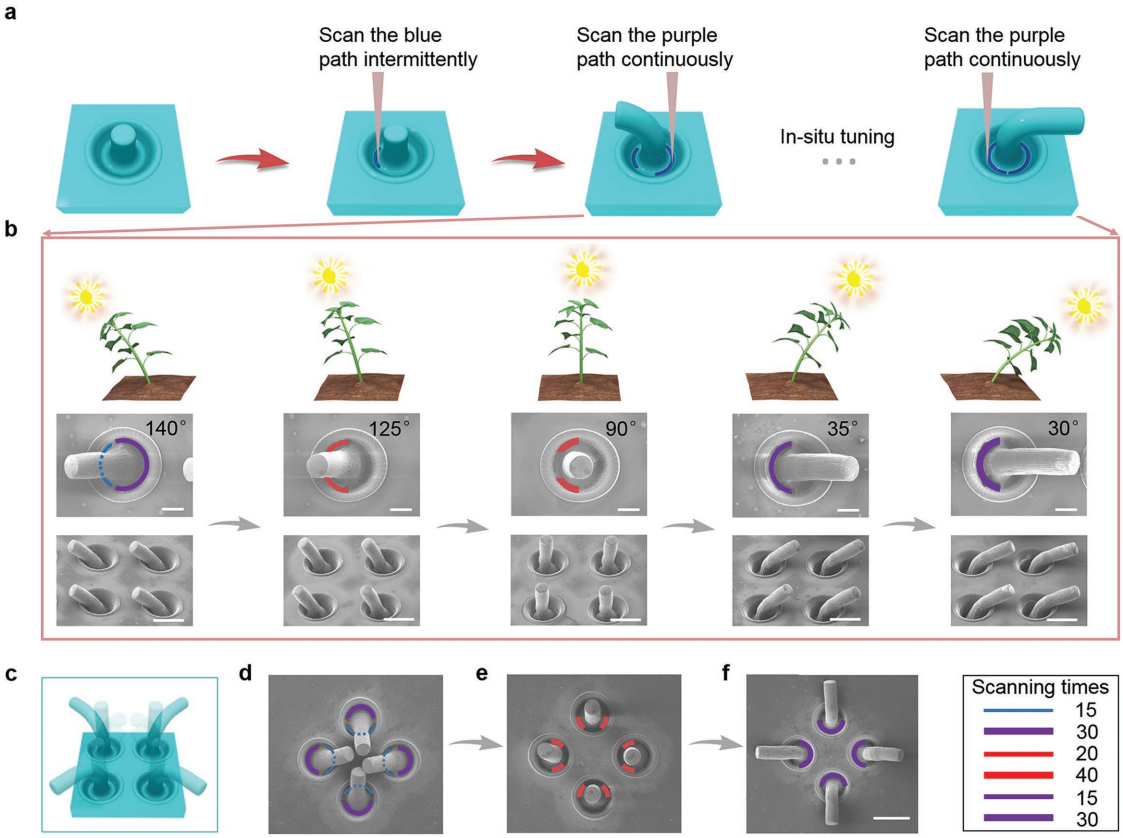

Figure 4. In situ tuning process of micropillar. a) Schematic of in situ tuning process. b) SEM images show the evolution of bent micropillar from left to right by in situ tuning mimicking the sunflower. Middle row are enlarged top view. Scale bars are 200 µm. Lower row are 45°-titled view. Scale bars: 500 µm. c) The schematic of claw-like structure from close state to open state by in situ tuning. d–f) The evolution of the claw-like structure from close state to open state by in situ tuning. Scale bars: 500 µm. Numbers in the legend show the repeat times of scribing for different scanning sequence and scanning path.

The pattern can still be distinguished with a reduced clarity (also see Figure S16, Supporting Information). Second, the pillars are bent to different directions. The ink on the top of the pillar deviates from their original site and the information is temporarily concealed (Figure S17 and Video S6, Supporting Information). Finally, the bent pillars return to the straight site when they are heated with a hot air gun and therefore the QR code can be recognized successfully again (Video S6, Supporting Information).

Similarly, color images can be encrypted and decrypted, e.g., "lips" as shown in Figure 5f. Furthermore, after shrinkage the ink on the top of micropillar is condensed thus the light-red lip turns to be dark red.

In summary, we propose a polymer self-growing method for constructing reconfigurable architectures on smart surface. We first observe the self-growing effect induced by laser scanning on SMP surface. We investigate the mechanisms underlying this novel phenomenon by introducing an improved shrinkage-growth model. By taking full advantage of the flexibility of laser writing, various straight micropillars with different cross-sections can be readily fabricated. Bent micropillars can be formed and assembled into complex surface patterns by utilizing asymmetric scanning strategy. Furthermore, the fabricated micropillar can be repeatedly tuned. Our structures suggest potential applications in the microparticle capture/release and information encryption, as demonstrated with the proof-of-concept experiments. The method of combined femtosecond laser direct writing and localized heating of SMP film opens up a new avenue to fabricate functional microstructures with great scalability and flexibility toward numerous applications in anti-counterfeiting, microstructure printing, and ultrasensitive detection.

Experimental Section

Materials and Equipment: The prestretched polystyrene film was purchased from Dongguan Nogard Arts & Crafts Factory. A differential scanning calorimeter Q2000 from TA Instrument was used to measure the glass transition temperature (T_g) of the film. The polystyrene microsphere used in the experiment was purchased from Knowledge & Benefit Sphere Tech. Co., Ltd, whose diameter was ranging from 150 to 200 µm. The microsphere was scattered on the surface of polystyrene film randomly before the fabrication. A CCD (Mindvision) with a macrolens is used to find the microsphere and locate the position of the micropillar in the microsphere capture experiment, it is also used to record the micropillar fabrication process and take pictures. In the information encryption experiment, the PS film surface is polished to facilitate printing. The QR code was generated by means of a free application accessible through the website http://cli.im/, using the error

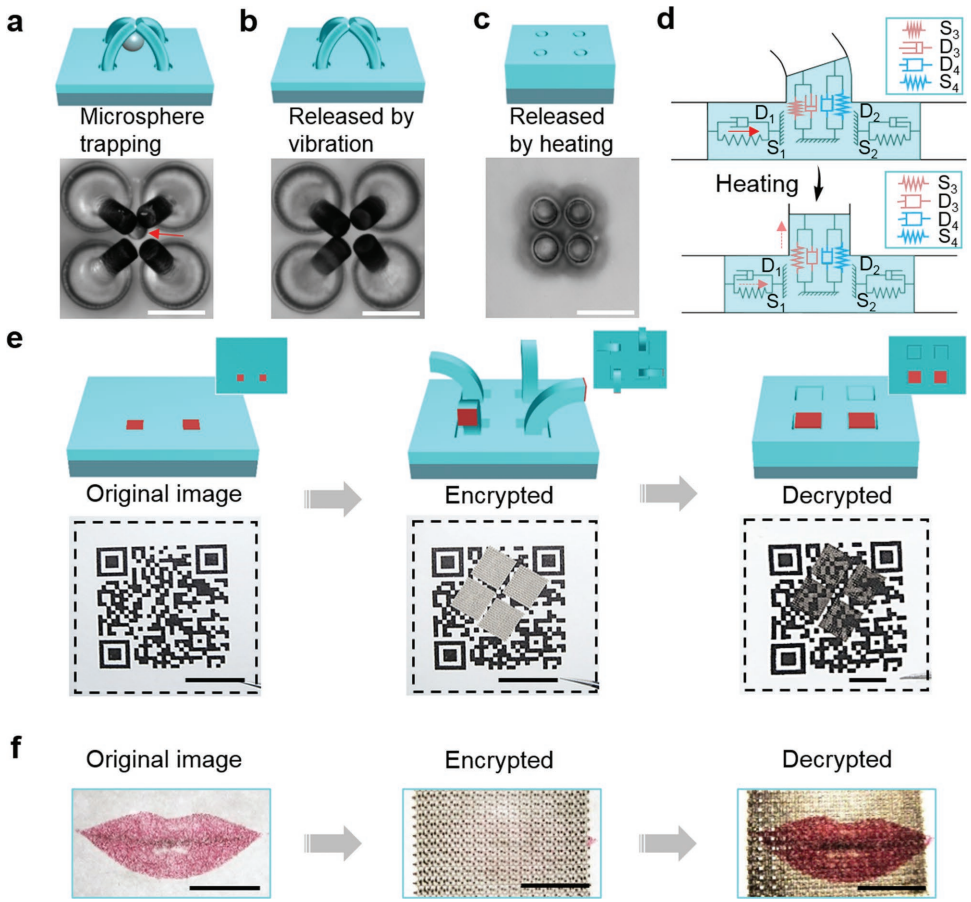

Figure 5. Applications of ALIPS-prepared structures on micro-object capture and information encryption. a) The claw-like structure captures one microsphere. b) Microsphere is released by vibration. c) Microsphere is released by heating the structure. Scale bars: 500 µm. d) Bend-recovery model of overall heating. e) Left: original QR code is printed on the polished surface. Middle: bent micropillars with different directions are fabricated on the part of the QR code. Right: information is decrypted after shrinkage. Information printed on the surface indicates as red in the corresponding schematic. Scale bars are 2, 2, and 0.5 cm, respectively. f) Encryption and decryption of color image. Scale bars are 5, 5, and 2 mm.

correction level "30%." The QR code were sent to the printer (Cannon, LBP6230dw) and printed on the PS film.

Femtosecond Laser Fabrication Method: A regenerative amplified Ti:sapphire femtosecond laser system (Legend Elite-1K-HE, Coherent, USA) with 104 fs pulse width, 1 kHz repetition rate and 800 nm central wavelength was employed to fabricate microstructures on the polystyrene film. The linearly polarized laser beam was guided onto the polystyrene film surface by a galvoscanner system (SCANLAB, Germany) equipped with a telecentric *f*-theta lens with a focal length of 63 mm. The height of the sample stage was adjusted to ensure the laser focus on the surface of the sample. The diameter of the focused spot is ≈20 µm. The scanning path was drawn by AutoCAD 2014 and saved as dxf file. Then the dxf file was imported into the processing software (Samlight). The scanning sequence was the same as the drawing sequence and could also be changed. The pulse energy was adjusted using a combination of a half-wave plate and a low dispersion polarizer. The scanning speed and repeat circles were controlled by the software Samlight.

Characterization: The SEM images was taken with a secondary electron scanning electron microscope (FEI, Sirion200) operated at 10 kV, after the samples were sputter coated with Au for 120 s. Optical microscope (LW200-3JT) was used to observe the side view of the micropillars. To quantitatively characterize the spectral responsivity, the wavelength dependence of absorbance in the UV, visible, and IR regions (200–1000 nm) was measured by a spectrophotometer (SOLID3700, Shimadzu, Japan). The photographs of the PS film during the shrinkage process were taken by a digital camera (PowerShot SX600HS, Cannon, Japan).

Supporting Information

Supporting Information is available from the Wiley Online Library or from the author.

Acknowledgements

This work was supported by the National Science Foundation of China (Nos. 51875544, 61475149, 51675503, 61805230, 51805508, 51805509), the Fundamental Research Funds for the Central Universities (WK 2090090012, WK2480000002, WK2090090021), Youth Innovation Promotion Association CAS (2017495), and National Key R&D Program of China (2018YFB1105400). This work was carried out at USTC Experimental Center of Engineering and Material Sciences. The authors thank Mr. Wulin Zhu for his contribution in the maintenance of the ultrafast lasers and establishment of the laser fabrication system.

Conflict of Interest

The authors declare no conflict of interest.

Keywords

femtosecond lasers, polymer self-growth, reconfigurable architectures, shape-memory polymers, shape transformation

Received: May 14, 2018
Revised: August 3, 2018
Published online: September 27, 2018

[1] C. Dawson, J. F. Vincent, A.-M. Rocca, *Nature* **1997**, *390*, 668.
[2] Y. Forterre, J. M. Skotheim, J. Dumais, L. Mahadevan, *Nature* **2005**, *433*, 421.
[3] R. Elbaum, L. Zaltzman, I. Burgert, P. Fratzl, *Science* **2007**, *316*, 884.
[4] H. Liang, L. Mahadevan, *Proc. Natl. Acad. Sci. USA* **2011**, *108*, 5516.
[5] J. J. Allen, G. R. Bell, A. M. Kuzirian, R. T. Hanlon, *J. Morphol.* **2013**, *274*, 645.
[6] C. Darwin, *The Power of Movement in Plants*, John Murray, London, UK **1880**.
[7] J. P. Vandenbrink, E. A. Brown, S. L. Harmer, B. K. Blackman, *Plant Sci.* **2014**, *224*, 20.
[8] L. Ionov, *J. Mater. Chem.* **2012**, *22*, 19366.
[9] R. Kempaiah, Z. Nie, *J. Mater. Chem. B* **2014**, *2*, 2357.
[10] S. Janbaz, R. Hedayati, A. Zadpoor, *Mater. Horiz.* **2016**, *3*, 536.
[11] Y. Liu, J. Genzer, M. D. Dickey, *Prog. Polym. Sci.* **2016**, *52*, 79.
[12] Z. Hu, X. Zhang, Y. Li, *Science* **1995**, *269*, 525.
[13] N. Bassik, B. T. Abebe, K. E. Laflin, D. H. Gracias, *Polymer* **2010**, *51*, 6093.
[14] J. Kim, J. A. Hanna, M. Byun, C. D. Santangelo, R. C. Hayward, *Science* **2012**, *335*, 1201.
[15] H. l. Thérien-Aubin, Z. L. Wu, Z. Nie, E. Kumacheva, *J. Am. Chem. Soc.* **2013**, *135*, 4834.
[16] Z. L. Wu, M. Moshe, J. Greener, H. Therien-Aubin, Z. Nie, E. Sharon, E. Kumacheva, *Nat. Commun.* **2013**, *4*, 1586.
[17] R. M. Erb, J. S. Sander, R. Grisch, A. R. Studart, *Nat. Commun.* **2013**, *4*, 1712.
[18] A. S. Gladman, E. A. Matsumoto, R. G. Nuzzo, L. Mahadevan, J. A. Lewis, *Nat. Mater.* **2016**, *15*, 413.
[19] T. Ikeda, M. Nakano, Y. Yu, O. Tsutsumi, A. Kanazawa, *Adv. Mater.* **2003**, *15*, 201.
[20] Y. Yu, M. Nakano, T. Ikeda, *Nature* **2003**, *425*, 145.
[21] T. J. White, D. J. Broer, *Nat. Mater.* **2015**, *14*, 1087.
[22] J.-a. Lv, Y. Liu, J. Wei, E. Chen, L. Qin, Y. Yu, *Nature* **2016**, *537*, 179.
[23] R. F. Shepherd, F. Ilievski, W. Choi, S. A. Morin, A. A. Stokes, A. D. Mazzeo, X. Chen, M. Wang, G. M. Whitesides, *Proc. Natl. Acad. Sci. USA* **2011**, *108*, 20400.
[24] R. V. Martinez, J. L. Branch, C. R. Fish, L. Jin, R. F. Shepherd, R. Nunes, Z. Suo, G. M. Whitesides, *Adv. Mater.* **2013**, *25*, 205.
[25] J. Pikul, S. Li, H. Bai, R. Hanlon, I. Cohen, R. Shepherd, *Science* **2017**, *358*, 210.
[26] J. Hu, H. Meng, G. Li, S. I. Ibekwe, *Smart Mater. Struct.* **2012**, *21*, 053001.
[27] R. Fernandes, D. H. Gracias, *Adv. Drug Delivery Rev.* **2012**, *64*, 1579.
[28] S. Felton, M. Tolley, E. Demaine, D. Rus, R. Wood, *Science* **2014**, *345*, 644.
[29] E. Wang, M. S. Desai, S.-W. Lee, *Nano Lett.* **2013**, *13*, 2826.
[30] Y. Liu, J. K. Boyles, J. Genzer, M. D. Dickey, *Soft Matter* **2012**, *8*, 1764.
[31] Y. Liu, M. Miskiewicz, M. J. Escuti, J. Genzer, M. D. Dickey, *J. Appl. Phys.* **2014**, *115*, 204911.
[32] Y. Liu, B. Shaw, M. D. Dickey, J. Genzer, *Sci. Adv.* **2017**, *3*, e1602417.
[33] B. Jin, H. Song, R. Jiang, J. Song, Q. Zhao, T. Xie, *Sci. Adv.* **2018**, *4*, eaao3865.
[34] C. S. Chen, D. N. Breslauer, J. I. Luna, A. Grimes, W. C. Chin, L. P. Lee, M. Khine, *Lab Chip* **2008**, *8*, 622.
[35] C.-C. Fu, A. Grimes, M. Long, C. G. L. Ferri, B. D. Rich, S. Ghosh, S. Ghosh, L. P. Lee, A. Gopinathan, M. Khine, *Adv. Mater.* **2009**, *21*, 4472.
[36] A. Chen, D. K. Lieu, L. Freschauf, V. Lew, H. Sharma, J. Wang, D. Nguyen, I. Karakikes, R. J. Hajjar, A. Gopinathan, *Adv. Mater.* **2011**, *23*, 5785.
[37] N. Liu, Q. Xie, W. M. Huang, S. J. Phee, N. Q. Guo, *J. Micromech. Microeng.* **2008**, *18*, 027001.
[38] W. K. Shih, *Polym. Eng. Sci.* **1994**, *34*, 1121.
[39] J. Morshedian, H. A. Khonakdar, S. Rasouli, *Macromol. Theory Simul.* **2005**, *14*, 428.

